IEEE Photonics Journal
An IEEE Photonics Society Publication

Open Access

Design of an Electro-Absorption Modulator Based on Graphene-on-Silicon Slot Waveguide

Volume 11, Number 3, June 2019

Lanting Ji
Daming Zhang
Yan Xu
Yang Gao
Chi Wu
Xibin Wang
Zhiyong Li
Xiaoqiang Sun

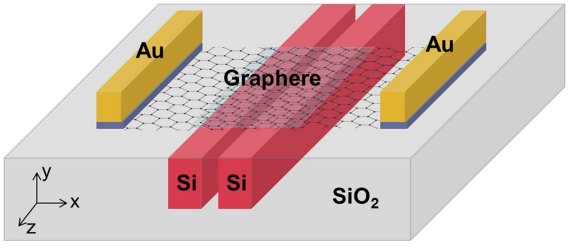

Configuration for optical modulator

DOI: 10.1109/JPHOT.2019.2918314
1943-0655

IEEE photonics SOCIETY

IEEE

Design of an Electro-Absorption Modulator Based on Graphene-on-Silicon Slot Waveguide

Lanting Ji,[1] Daming Zhang,[1] Yan Xu,[1] Yang Gao,[1] Chi Wu,[2] Xibin Wang,[1] Zhiyong Li,[3] and Xiaoqiang Sun [1]

[1]State Key Laboratory of Integrated Optoelectronics, College of Electronic Science and Engineering, Jilin University, Changchun 130012, China
[2]Institute of Marine Science and Technology, Shandong University, Qingdao 250100, China
[3]State Key Laboratory of Integrated Optoelectronics, Institute of Semiconductors, Chinese Academy of Sciences, Beijing 100083, China

DOI:10.1109/JPHOT.2019.2918314

Manuscript received April 26, 2019; accepted May 17, 2019. Date of publication May 22, 2019; date of current version May 30, 2019. This work was supported in part by the National Natural Science Foundation of China under Grants 61675087, 61575076, and 61605057; and in part by the National Key Research and Development Plan of China under Grant 2016YFB0402502. Corresponding author: Xiaoqiang Sun (e-mail: sunxq@jlu.edu.cn).

Abstract: Compact high-performance electro-optic (EO) modulators are key elements for optical communications. An electro-absorption modulator is theoretically designed. Due to the introduction of graphene film over the silicon slot waveguide, the modulation efficiency is strongly improved. The effect of waveguide dimensions, dielectric insulator thickness, and carrier mobility on performances of the proposed EO modulator have been comprehensively investigated. For the 120-μm-long graphene-on-silicon waveguide modulator, the extinction ratio 28 dB and insertion loss 1.28 dB can be obtained at 1550 nm when drive voltage is 1.91 and 0.59 V, respectively. The 3 dB bandwidth of 117 GHz can be obtained at a small power consumption of 212 fJ/bit. The proposed modulator possesses a high figure-of-merit of 20.5. Its benefits of small size, power saving, and process compatible promises possible applications in on-chip signal processing.

Index Terms: Waveguide modulators, integrated optics devices, electro-optical devices, graphene.

1. Introduction

Electro-Optic (EO) modulator is a crucial component for signal processing and optics communications. Silicon, InP, $LiNbO_3$, nonlinear polymers have been used in EO modulators construction to satisfy the requirements of fast response, wide optical bandwidth, compact size, low insertion loss, and power saving [1]–[7]. Electro-absorption (EA) EO modulators, such as Ge or SiGe modulators, have benefits of small size and broadband operation. However, they suffer from limited thermal ability and large insertion loss [8], [9]. As a promising optical material, graphene exhibits favorable characteristics of wide optical bandwidth, adjustable absorption, fast-speed modulating, and high nonlinearity [10]–[16], which are favorable to on-chip integration and low power consumption applications of EO modulator. However, the single-atom thickness of graphene leads to the weak interaction to vertical incident light. Certain optical structures are demanded to strengthen the influence of graphene flake (GF) on the mode field in waveguide, which results in a high modulation rate

by the graphene layer. Thereby, electro-refractive graphene-based waveguide modulators based on Mach-Zehnder interferometer, micro-ring and other structures have been theoretically investigated [15], [17]–[21]. However, the advantage of wide bandwidth of graphene is sacrificed for obtaining large extinction ratio and low power consumption. Comparatively, graphene-on-silicon (GoS) waveguide EA modulators hold more favourable characteristics of graphene [14], [22]–[29]. Liu *et al.* experimentally demonstrated a monolayer graphene EA modulator with a mode power attenuation (MPA) of 0.10 dB/μm [14]. Because of the adoption of double layer graphene, better MPA and modulation frequency performance of 0.16 dB/μm and 1.2 GHz at a low power consumption of 1 PJ/bit can be obtained [22]. Higher modulation speed of 10 Gb/s with a low power consumption of $\sim$350 fJ/bit and a low insertion loss of 3.8 dB for a hybrid graphene-Si EA modulator also has been reported [23]. However, perfect graphene model adopted in the theoretical study is not well in accordance with the practical modulating condition [15], [18]–[20], [25]–[27].

In this paper, practical factors have been considered and included in the design of a transverse electric (TE) mode GoS slot waveguide EA modulator. Effects of waveguide dimensions, quantum capacitance, carrier mobility, sidewall roughness, and carrier concentration operating range (Fermi energy, 0.3–0.6 eV) have been comprehensively investigated. The modulator consists of silica cladding, low-index slot formed by paralleled high refractive index silicon stripes and two GFs above the slot waveguide. With the influence of enhanced light-intensity in graphene, improved modulation efficiency is realized. Through optimizations of geometric parameter of GoS slot waveguide, the 120 μm-long GoS waveguide EO modulator demonstrates an extinction ratio of $\sim$28 dB, insertion loss of $\sim$1.28 dB, 3-dB bandwidth of $\sim$117 GHz, and power consumption of $\sim$212 fJ/bit.

2. Device Structure

The periodicity of graphene exists in the two-dimensional lattice plane. The variation of its chemical potentials μ_c (Fermi level) can actively tune its in-plane permittivity ($\varepsilon_{//}$), however, leading to unremarkable difference for the out-of-plane permittivity ($\varepsilon_{\perp}$). It is well known that the complex optical conductivity of graphene is mainly determined by μ_c, optical frequency (ω), charged particle scattering rate Γ ($\Gamma = 1/\tau$, where τ corresponds to relaxation time), as well as temperature (T). The interband and intraband transitions that contribute to the complex optical conductivity of graphene can be expressed as [30], [31]

$$\sigma_{//} = \sigma_{intra} + \sigma'_{inter} + j\sigma''_{inter} \tag{1}$$

where

$$\sigma_{intra} = \sigma_0 \frac{4\mu_c}{\pi} \frac{1}{\hbar(\Gamma_1 - j\omega)} \tag{2}$$

$$\sigma'_{inter} = \sigma_0 \left[1 + \frac{1}{\pi}\tan^{-1}\left(\frac{\hbar\omega - 2\mu_c}{\hbar\Gamma_2}\right) - \frac{1}{\pi}\tan^{-1}\left(\frac{\hbar\omega + 2\mu_c}{\hbar\Gamma_2}\right)\right] \tag{3}$$

$$\sigma''_{inter} = -\sigma_0 \frac{1}{2\pi} \ln\left[\frac{(2\mu_c + \hbar\omega)^2 + (\hbar\Gamma_2)^2}{(2\mu_c - \hbar\omega)^2 + (\hbar\Gamma_2)^2}\right] \tag{4}$$

where $\hbar$ is the reduced Planck's constant, $\sigma_0 \approx 60.8$ μS is the universal optical conductance, τ_1 of 1.2 ps is related to intraband transitions [19], and τ_2 of 15 fs is related to interband transitions [32]. In practical application, modulators are supposed to work at room temperature. Therefore, both relaxation times are adopted at the room temperature ($T = 300$ K) in this work. The in-plane permittivity $\varepsilon_{//}$ then can be obtained from [14], [30]

$$\varepsilon_{//}(\omega) = 2.5 + \frac{j\sigma_{//}(\omega)}{\omega\varepsilon_0 d} \tag{5}$$

where ε_0 is the permittivity of vacuum. The graphene thickness d is selected as 0.7 nm in the simulation [20]. Figure 1(a) shows $\varepsilon_{//}$ change of graphene with its μ_c when λ is 1550 nm. The

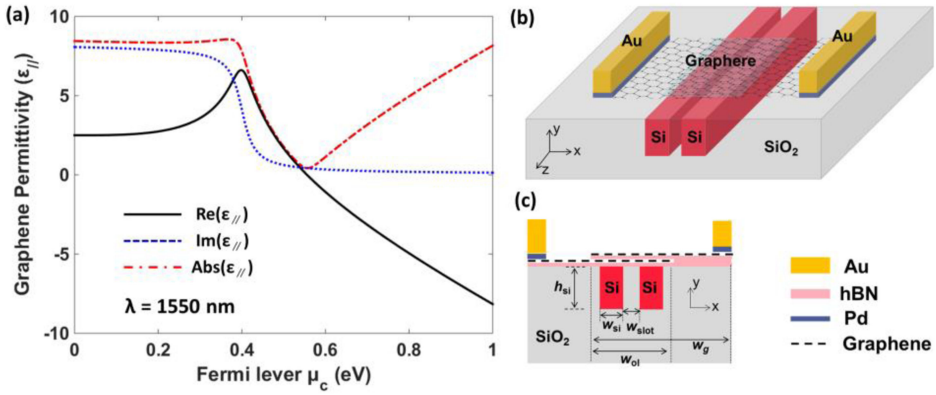

Fig. 1. (a) In-plane ε_g changes with μ_c of graphene when λ is 1550 nm (at room temperature 300 K). (b) 3-D schematic diagram. (c) Cross section of proposed waveguide.

imaginary part of $\varepsilon_{//}$ (Im($\varepsilon_{//}$)) decreases significantly as μ_c shifts from 0.35 to 0.45 eV. According to the working principle of GoS waveguide modulator, Re($\varepsilon_{//}$) and Im($\varepsilon_{//}$) of graphene may be effectively adjusted by tuning μ_c, then determined by the waveguide effective index (N_{eff}). Since the imaginary part of N_{eff} (Im(N_{eff})) decided by the optical propagation attenuation, the relationship between MPA and Im(N_{eff}) can be described as

$$MPA = 40\pi \left(log_{10} e\right) Im\left(N_{eff}\right)/\lambda \tag{6}$$

Due to the anisotropy of graphene, ($\varepsilon_\perp$) stays constantly at 2.5 [33], [34]. Therefore, the permittivity of graphene (ε_g) may be expressed as

$$\hat{\varepsilon}_g = \begin{pmatrix} \varepsilon_{//} & 0 & 0 \\ 0 & 2.5 & 0 \\ 0 & 0 & \varepsilon_{//} \end{pmatrix} \tag{7}$$

The proposed GoS waveguide modulator consists of the silica cladding, low-index slot waveguide formed by two paralleled high refractive index silicon stripes, and two GFs above the slot waveguide. As shown in Fig. 1(b), the hBN (Hexagonal boron nitride) layer is adopted to stop carriers diffusing. Meanwhile, these two GFs separated by the hBN layer forms a slab capacitor. The hBN exhibits unique electronic properties, such as wide bandgap, large transparency window, low dielectric constant and chemical inertness [35]. The hexagonal structure of hBN makes its lattice matching well with graphene [36]. Due to the low resistance of Pd/graphene contact, the metal palladium followed by Au are formed as electrodes [37]. The slot silicon waveguides surrounded by silica can be fabricated by using standard CMOS technologies, including electron-beam lithography (EBL), chemical vapor deposition (CVD), and sequential chemical–mechanical polishing [38]–[40]. The stack structure of graphene/hBN may be formed by sequentially depositing h-BN via ion beam sputtering deposition (IBSD) and graphene with CVD method [41], [42], Then the graphene-hBN-graphene stack is transferred onto the top of slot waveguide [41], [43]. The graphene pattern can be defined by ultraviolet lithography and oxygen plasma etching. Au/Pd contacts is formed by Au/Pd metal deposition and liftoff process [41], [44]. In Fig. 1(c), w_{slot}, h_{si}, and w_{si} represent the slot width of GoS, the height and width of silicon waveguide, respectively. Here, L and w_g correspond to the length and effective width of graphene, respectively. While, w_{ol} refers to the common width between two graphene layers. To reduce the optical loss caused by metal contacts and the resistance outside the capacitance structure, w_{ol} and w_g are chosen to be 1.1 and 1.8 μm, respectively [32]. The indices of silica, silicon, as well as hBN are assumed to be 1.44, 3.47, and 1.98, respectively. Following simulations are performed by using the finite-element method.

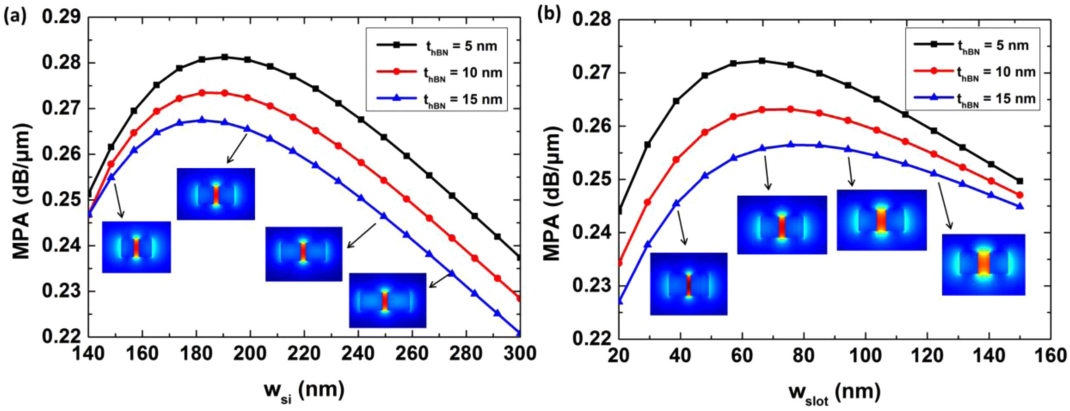

Fig. 2. Optical power attenuation of fundamental TE polarization mode as a function of (a) w_{si}, and (b) w_{slot} when μ_c is 0 eV under different thickness of hBN layer. The insets are the corresponding mode field distributions of GoS waveguides.

3. Modulator Design

3.1 Effect of GoS Waveguide Dimensions

To confirm the configuration of proposed modulator, the impact of geometric dimensions on the attenuation of GoS waveguide is evaluated at 1550 nm, because higher MPA implies stronger reciprocal action between the optical field and GFs. According to standard silicon process, the height of silicon waveguide h_{si} is firstly set to be 220 nm. When w_{slot} is 60 nm, the impact of w_{si} on the MPA of fundamental TE polarization at neutrality point ($\mu_c = 0$ eV) is investigated. The thickness of hBN insulator is chosen to be 5, 10, and 15 nm, respectively. As shown in Fig. 2(a), MPA primarily rises when w_{si} is lower than 190 nm. When w_{si} is over 190 nm, MPA gradually decreases. The largest absorption reaches 0.283 dB/μm when w_{si} and t_{hBN} are 190 and 5 nm, respectively. Therefore, w_{si} is chosen to be 190 nm. When w_{si} is fixed at 190 nm, the MPA in GoS waveguide versus w_{slot} at $\mu_c = 0$ eV is shown in Fig. 2(b). The attenuation of GoS waveguide firstly increases to a maximum value when w_{slot} is close to 65 nm, and then decreases with the increment of w_{slot}. Hence, the w_{slot} is chosen as 65 nm to obtain a high MPA, meanwhile maintaining a high optical field density in the nanometer slot. As shown in Fig. 2, the GoS waveguide with 5 nm-thick hBN has a relatively larger attenuation than that with 10 nm- or 15 nm-thick hBN, which means a thinner hBN layer leads to a stronger reciprocal action between GFs and the optical field. The insets are corresponding mode field distributions in the GoS waveguide. The optical mode is well confined in the nanometer slot.

3.2 Effect of Fermi Level

According to calculations in Section 3.1, the geometric parameters $h_{si} = 220$ nm, $w_{si} = 190$ nm and $w_{slot} = 65$ nm for the GoS waveguide are adopted in the following work. The relationship between the real part of effective mode index Re(N_{eff}), the imaginary part of effective mode index Im(N_{eff}), and μ_c of graphene under different hBN thicknesses are investigated. As shown in Fig. 3(a), under different hBN thicknesses of 5, 10, and 15 nm, Re(N_{eff}) varies 0.0140, 0.0135, and 0.0131, respectively, as μ_c increases from 0.408 to 1 eV. As shown in Fig. 3(b), when $\mu_c = 0$ eV, the maximum Im(N_{eff}) is 0.00773, 0.00747, and 0.00726, respectively, under different hBN thicknesses of 5, 10, and 15 nm. The minimum Im(N_{eff}) is 1.386×10^{-4}, 1.330×10^{-4}, and 1.288×10^{-4}, respectively, for different t_{hBN} at $\mu_c = 1$ eV. This can be explained that both the effective mode index variation and attenuation increase with the reduction of insulating layer thickness t_{hBN}, which is induced by the enhancement of reciprocal action between GFs and the optical field. However, the thickness of isolation layer is not desired to be too small, because of the possible breaking down of graphene capacitor.

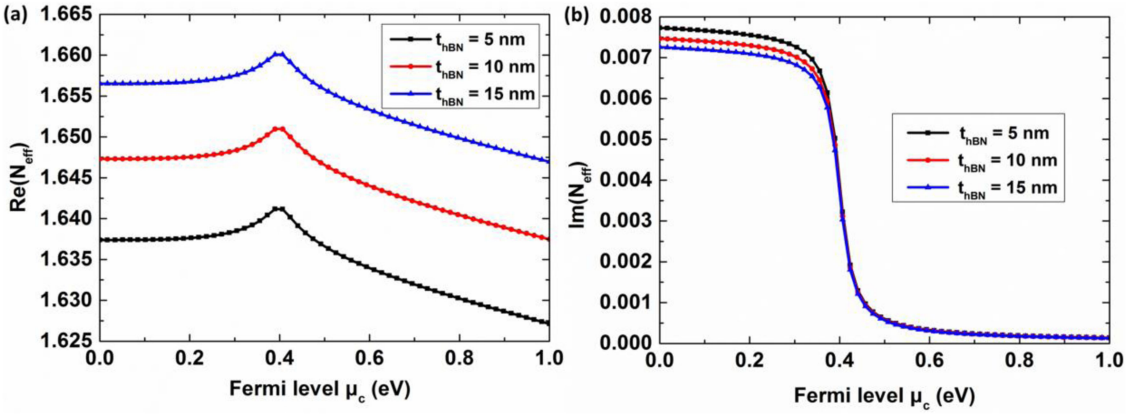

Fig. 3. (a) Re(N_{eff}) and (b) Im(N_{eff}) of fundamental TE mode as a function of μ_c under different hBN thicknesses ($\tau = 15$ fs).

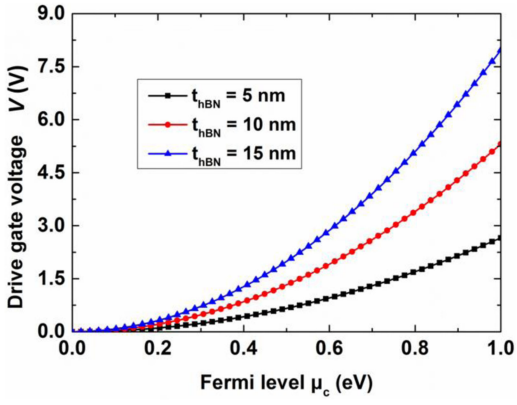

Fig. 4. The relationship between V and μ_c under different hBN thicknesses of 5, 10, and 15 nm.

3.3 Effect of Drive Gate Voltage

To reasonably confirm the thickness of hBN layer, the relationship between the drive gate voltage and μ_c of graphene has been investigated. Assuming a gate voltage is applied to one GF, while another GF is grounded, μ_c of graphene could be tuned based on the following equation [45], [46]

$$|\mu_c| = \hbar v_F \sqrt{\pi \eta \left| V_g - V_0 \right|} \tag{8}$$

where $v_F = 2.5 \times 10^6$ m/s is the Fermi velocity of graphene [47], η can be generated from $\varepsilon_r \varepsilon_0 / t_{\text{hBN}} e$, t_{hBN} is the separation distance between two graphene plates by hBN. For simplicity, $|V_g - V_0|$ as a whole can be regarded as the applied gate voltage V. Figure 4 demonstrates the relationship between V and μ_c. For practical application, the GoS waveguide modulator should operate at room temperature, therefore, the variation range of chemical potential of graphene is chosen to be from 0.3 to 0.6 eV, but not from 0 to 1 eV. The driving voltage change under different t_{hBN} of 5, 10, and 15 nm are 0.74, 1.47 and 2.25 V, respectively. The drive gate voltages at $\mu_c = 0.6$ eV for different t_{hBN} are 0.99, 1.99 and 2.98 V, respectively. According to Ref. [48], these three drive gate voltages are all smaller than theoretical breakdown voltages of 5, 9, and 13 V for hBN layer with thickness of 5, 10, and 15 nm, respectively. Hence, the hBN isolation layer with these three supposed thicknesses can be applied in EA modulator design.

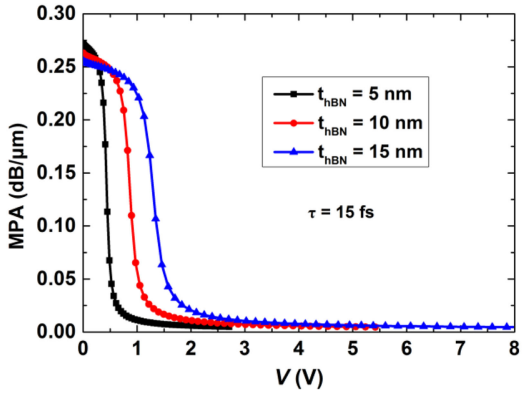

Fig. 5. The mode power attenuation changes with the drive gate voltage under different hBN thicknesses.

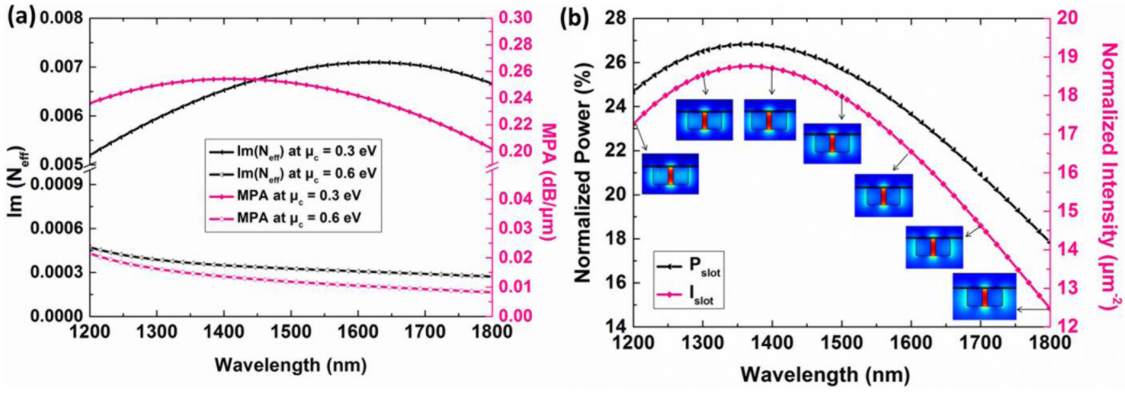

Fig. 6. (a) MPA and Im(N_{eff}) as a function of optical wavelength at different μ_c of 0.3 and 0.6 eV, and (b) wavelength dependence of P_{slot} and I_{slot} in the slot waveguide.

The MPA of fundamental TE mode changing with the drive gate voltage under different hBN thicknesses is shown in Fig. 5. To realize the same attenuation, the required drive gate voltage decreases with the decrement of hBN thickness. Under t_{hBN} of 5, 10, and 15 nm, the MPA shows a maximum attenuation ($\mu_c = 0$ eV) of 0.272, 0.263, and 0.255 dB/μm, respectively. Comprehensively considering the impact of hBN thickness change on the effective mode index, gate voltage and attenuation, the thickness of hBN is chosen to be 10 nm.

4. Results and Discussion

Based on above analysis, design parameters of EA modulator are $h_{si} = 180$ nm, $w_{si} = 220$ nm, $w_{slot} = 70$ nm, $t_{hBN} = 10$ nm, $\tau = 15$ fs, $V = 1.99$ V, $w_{ol} = 1.1$ μm and $w_g = 1.8$ μm. To comprehend the modulation performance with proposed parameters, the MPA dependence on wavelength, FoM dependence on gate voltage, power consumption and frequency response are investigated.

4.1 MPA and Im(N_{eff}) Dependence on Wavelength

The wavelength dependence of Im(N_{eff}) and MPA when μ_c is 0.3 and 0.6 eV is shown in Fig. 6(a). When λ varies from 1200 to 1615 nm, Im(N_{eff}) grows gradually from 0.00519 to 0.0071 when μ_c is 0.3 eV. When μ_c is 0.6 eV, the Im(N_{eff}) is in the 10^{-4} orders of magnitude. Different from Im(N_{eff}), MPA decreases slightly from 0.254 to 0.202 dB/μm as λ varies from 1415 to 1800 nm

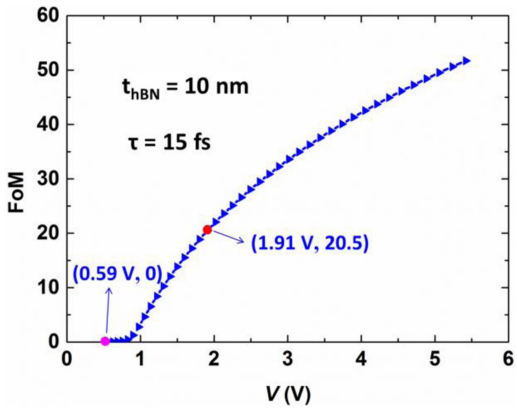

Fig. 7. FoM as a function of drive gate voltages when the hBN thickness is 10 nm and relaxation time is 15 fs.

when μ_c is 0.3 eV. When μ_c is 0.6 eV, the MPA value is smaller than 0.02 in the 1×10^{-2} orders of magnitude within the wavelength range from 1200 to 1600 nm. The wavelength dependence of normalized optical power P_{slot} and normalized average optical intensity I_{slot} in the nanoscale slot is shown in Fig. 6(b). It is clear that the P_{slot} and I_{slot} vary less than 10% over a wavelength span of 600 nm. The slot structure shows low wavelength sensitivity because its eigenmode can be seen as the interaction of fundamental eigenmodes of two slab waveguides and no interference effect is involved in the guiding and confinement mechanism [49]. The independence of MPA on wavelength promises a broad operation bandwidth for proposed modulator.

4.2 FoM Dependence on Drive Gate Voltage

The FoM (extinction ratio/insertion loss) is adopted to access the operation of an EA modulator. The relationship between FoM and drive gate voltage is investigated when relaxation time is 15 fs and hBN thicknesses is 10 nm, as shown in Fig. 7. FoM grows rapidly when V is larger than 1 V. It can be as high as 52 when the drive gate voltage is 5.3 V. For practical room temperature working consideration, a high FoM of 20.5 can be obtained at gate voltage of 1.91 V, which corresponds to the upper Fermi level 0.6 eV within the operating region.

4.3 Insertion Loss and Extinction Ratio Dependence on Graphene Length

For EA modulators, the length of the device greatly affects the insertion loss and extinction ratio. We investigate the dependence of insertion loss and extinction ratio of the proposed modulator on the graphene length L. As shown in Fig. 8, the insertion loss, as well as the extinction ratio, increases with the increment of graphene length at a rate of 0.01 and 0.236 dB/μm, respectively, when $t_{hBN} = 10$ nm and $\tau = 15$ fs. Here, L of 120 μm is chosen to obtain an extinction ratio of 28 dB and an insertion loss of 1.28 dB. It should be noted that the silicon slot waveguide sidewall roughness, which will lead to scattering loss, is unavoidable in fabrication process. The sidewall roughness as a series of non-uniform variation of waveguide width, can be seen as gratings with different periods and modulation depths along the waveguide direction, which will couple the forward-propagating optical mode to radiation and backward-propagating mode, inducing back-scattering loss [50], [51]. Different methods, including thermal oxidation with oxygen gas and steam, anisotropic wet etching with tetramethylammonium hydroxide [52], and thermal annealing in hydrogen [53] have been proposed to reduce the surface roughness of silicon waveguide. Especially, the loss of 4.6 dB/cm for TE polarization slot waveguide has been realized by standard wet chemical wafer cleaning process [54]. Assuming the loss coefficient of the silicon slot waveguide is around 5 dB/cm according to the

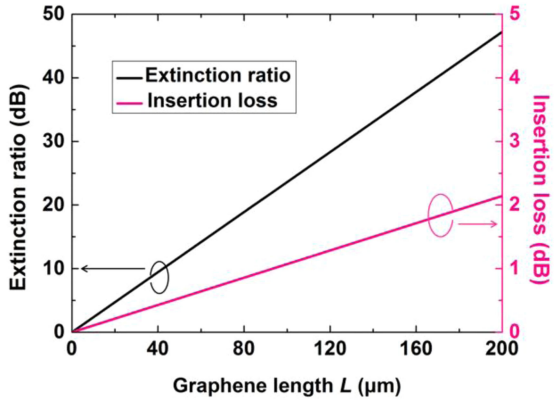

Fig. 8. Insertion loss and extinction ratio as a function of the graphene length.

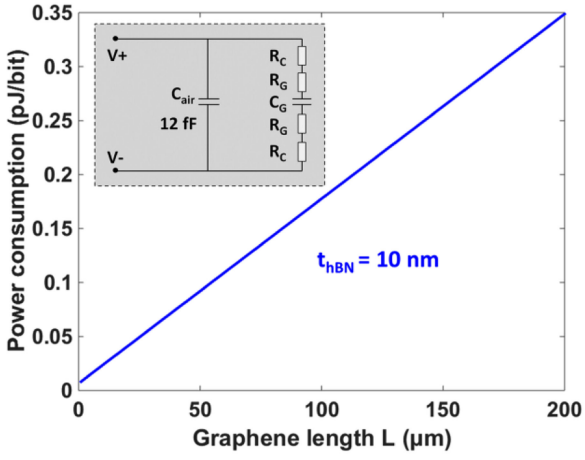

Fig. 9. Power consumption as a function of graphene length.

reported results [54]–[58], for the designed 120 μm-long EA graphene modulator, the loss caused by sidewall roughness can be reduced to 0.06 dB. It contributes only 4.5% of the total transmission loss. This low loss is supposed to have inconspicuous impact on the modulating performance of proposed design. This low loss is supposed to have inconspicuous impact on the modulating performance of proposed design.

4.4 Power Consumption and Frequency Response

As key parameters of EO modulators, power consumption and frequency response largely determine the application of proposed design. Therefore, an equivalent electrical circuit model is used to investigate the frequency response of proposed modulator, as shown in the inset of Fig. 9. The capacitance C_{air} formed by the air between the two electrodes is about 12 fF [35]. The capacitance C_G originating from the stack of graphene-hBN-graphene includes dielectric capacitance C_D and quantum capacitance C_Q. The quantum capacitance $C_Q = C_{q0} w_{ol} L$ is a series capacitance, which contributes to the reduction of total capacitance as well as the resulted faster speed. Where, C_{q0} presents the charge variation induced by gate voltage, and can be calculated by [59]

$$C_{q0} = \frac{2q^2 kT}{\pi(\hbar v_F)^2} \ln\left[2\left(1 + \cosh\frac{qV_{ch}}{kT}\right)\right] \tag{9}$$

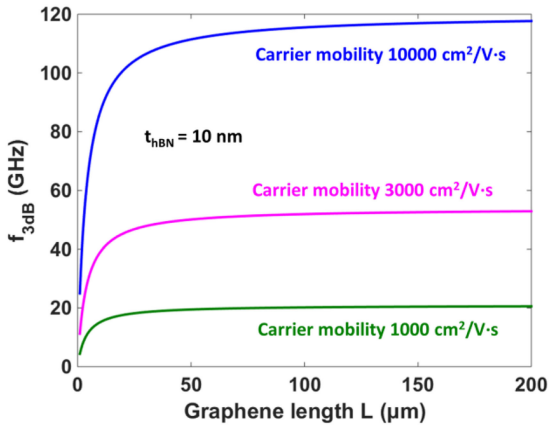

Fig. 10. The 3-dB bandwidth of proposed modulator as a function of graphene length.

where v_F is the Fermi velocity of graphene, q is the electron charge, $qV_{ch} = \mu_c$ is the Fermi level at room temperature of 300 K, $\hbar$ is the reduced Planck's constant, k is the boltzmann constant. The average C_{q0} is calculated to be $\sim$1.5067 μF/cm^2 by integrating C_G over the applied gate voltage ranging from 0.59 to 1.91 V and the supposed background doping level of $n_b = 9 \times 10^{12}$ cm^{-2} [60]. Dielectric capacitance C_D can be written as

$$C_D = \varepsilon_r \varepsilon_0 w_{ol} L / t \tag{10}$$

The power consumption then can be estimated based on equation

$$E_{bit} = C(\Delta U)^2/4 \tag{11}$$

where $C = C_{air} + C_D + C_Q$ is the total capacitance of the circuit. The power consumption as a function of graphene length L is shown in Fig. 9. The power consumption linearly increases with the graphene length. When L is 120 μm, the power consumption is as low as 212 fJ/bit. However, to ultimately confirm the graphene length, the frequency response dependence on graphene length is supposed to be studied.

As has been reported, the 3-dB bandwidth f_{3dB} can be evaluated by [61]

$$f_{3\,dB} = \frac{1}{2\pi RC} \tag{12}$$

The series resistance R consisting of graphene sheet resistance R_G and P$_d$/graphene contact resistance R_C can be expressed as [60], [62]

$$R = 2R_{g,s} \cdot \frac{w_g}{L} + \frac{2R_{g,c}}{L} \tag{13}$$

where $R_{g,c} = 100\ \Omega \cdot \mu$m is the contact resistance [37]. To study the impact of carrier mobility on the 3-dB bandwidth, three sheet resistance $R_{g,s}$ of 69, 230, and 690 $\Omega/\square$ that corresponds to carrier mobilities of 10000, 3000, and 1000 cm^2/V·s, respectively, have been selected in the calculation of f_{3dB} as a function of graphene length [32], as shown in Fig. 10. It can be seen that the carrier mobility has a remarkable influence on the 3-dB bandwidth. A higher carrier mobility gives rise to a larger f_{3dB}. Besides, f_{3dB} gradually saturates and almost remains at a certain level for all carrier mobilities, when the graphene length is larger than 20 μm. This implies the selection of graphene length mainly depends on the power consumption, insertion loss and extinction ratio. Therefore, when L is 120 μm, for the carrier mobility of 10000 cm^2/V·s, the f_{3dB} is $\sim$117 GHz.

5. Conclusions

In summary, a GoS waveguide EO modulator is designed and investigated. With the introduction of silicon slot waveguide, the reciprocal action between the optical field and GFs is effectively improved. Impact of waveguide dimensions, dielectric insulator thickness, and carrier mobility on the performance of modulator have been investigated and discussed, too. Simulation results show that the 120 μm-long GoS waveguide EO modulator presents an extinction ratio of 28 dB and an insertion loss of 1.28 dB at the optical wavelength of 1550 nm. The 3-dB bandwidth is around 117 GHz at a low power dissipation of 212 fJ/bit. The proposed design with a FoM of 20.5 is footprint-compact, energy-efficient, low insertion loss and technology compatible.

References

[1] Q. Xu, B. Schmidt, S. Pradhan, and M. Lipson, "Micrometre-scale silicon electro-optic modulator," *Nature*, vol. 435, no. 1, pp. 325–327, May 2005.

[2] H. Mohseni, H. An, Z. A. Shellenbarger, M. H. Kwakernaak, and J. H. Abeles, "Enhanced electro-optic effect in GaInAsP–InP three-step quantum wells," *Appl. Phys. Lett.*, vol. 84, no. 11, pp. 1823–1825, Mar. 2003.

[3] D. Janner *et al.*, "Very low voltage single drive domain inverted $LiNbO_3$ integrated electro-optic modulator," *Opt. Exp.*, vol. 15, no. 17, pp. 10739–10743, Aug. 2007.

[4] F. Qiu *et al.*, "A hybrid electro-optic polymer and TiO2 double-slot waveguide modulator," *Sci. Rep.* vol. 5, Feb. 2015, Art. no. 8561.

[5] X. Sun *et al.*, "Effect of film compatibility on electro-optic properties of dye doped polymer DR1/SU-8," *Appl. Surf. Sci.*, vol. 285, pp. 469–476, Aug. 2013.

[6] X. L. Zhao *et al.*, "Optimized design and fabrication of nanosecond response electro-optic switch based on ultraviolet-curable polymers," *Chin. Phys. B*, vol. 24, no. 4, Feb. 2015, Art. no. 044101.

[7] X. B. Wang *et al.*, "Performance enhancement of strip-loaded electro-optic modulator using photobleaching-assisted method," *Appl. Phys. B*, vol. 118, no. 4, pp. 579–585, Feb. 2015.

[8] A. V. Krishnamoorthy *et al.*, "High speed GeSi electro-absorption modulator at 1550 nm wavelength on SOI waveguide," *Opt. Exp.*, vol. 20, no. 20, pp. 22224–22232, Sep. 2012.

[9] M. H. Park, L. C. Wang, J. Cheng, and C. J. Palmstrm, "Low resistance Ohmic contact scheme ($\sim\mu\Omega$ cm^2) to p-InP," *Appl. Phys. Lett.*, vol. 70, no. 1, pp. 99–101, Jan. 1997.

[10] P. Avouris and M. Freitag, "Graphene photonics, plasmonics, and optoelectronics," *IEEE J. Sel. Topics Quantum Electron.*, vol. 20, no. 1, pp. 72–83, Jan./Feb. 2014.

[11] K. Shi, W. Zhao, and Z. Lu, "Greatly enhanced ultrabroadband light absorption by monolayer graphene," *Opt. Lett.*, vol. 38, no. 21, pp. 4342–4345, Nov. 2013.

[12] Z. Sun *et al.*, "Graphene mode-locked ultrafast laser," *ACS Nano*, vol. 4, no. 2, pp. 803–810, Jan. 2010.

[13] Z. Luo *et al.*, "Graphene-induced nonlinear four-wave-mixing and its application to multiwavelength Q-switched rare-earth-doped fiber lasers," *IEEE J. Lightw. Technol.*, vol. 29, no. 18, pp. 2732–2739, Sep. 2011.

[14] M. Liu *et al.*, "A graphene-based broadband optical modulator," *Nature*, vol. 474, no. 7349, pp. 64–67, Jun. 2011.

[15] L. Yang *et al.*, "Low-chirp high-extinction-ratio modulator based on graphene-silicon waveguide," *Opt. Lett.*, vol. 38, no. 14, pp. 2512–2515, Jul. 2013.

[16] D. A. Kuzmin, I. V. Bychkov, and V. G. Shavrov, "Influence of graphene coating on speckle-pattern rotation of light in gyrotropic optical fiber," *Opt. Lett.*, vol. 40, no. 6, pp. 890–893, Mar. 2015.

[17] C. Xu, Y. Jin, L. Yang, J. Yang, and X. Jiang, "Characteristics of electro-refractive modulating based on Graphene-Oxide-Silicon waveguide," *Opt. Exp.*, vol. 20, no. 20, pp. 22398–22405, Sep. 2012.

[18] R. Hao, W. Du, H. Chen, X. Jin, L. Yang, and E. Li, "Ultra-compact optical modulator by graphene induced electro-refraction effect," *Appl. Phys. Lett.*, vol. 103, no. 6, pp. 518–526, Aug. 2013.

[19] A. Phatak, C. Qin, K. Goda, and Z. Cheng, "Design of electro-optic modulators based on graphene-on-silicon slot waveguides," *Opt. Lett.*, vol. 41, no. 11, pp. 2501–2504, Jun. 2016.

[20] S. W. Ye, F. Yuan, X. H. Zou, M. K. Shah, R. G. Lu, and Y. Liu, "High-speed optical phase modulator based on graphene-silicon waveguide," *IEEE J. Sel. Topics Quant.*, vol. 23, no. 1, pp. 76–80, Jan. 2016.

[21] M. Mohsin *et al.*, "Experimental verification of electro-refractive phase modulation in graphene," *Sci. Rep.*, vol. 5, Mar. 2015, Art. no. 10967.

[22] M. Liu, X. Yin, and X. Zhang, "Double-layer graphene optical modulator," *Nano. Lett.*, vol. 12, no. 3, pp. 1482–1485, Feb. 2012.

[23] Y. Hu *et al.*, "Broadband 10 Gb/s operation of graphene electro-absorption modulator on silicon," *Laser Photon. Rev.*, vol. 10, no. 2, pp. 307–316, Mar. 2016.

[24] M. Mohsin, D. Schall, M. Otto, A. Noculak, D. Neumaier, and H. Kurz, "Graphene based low insertion loss electro-absorption modulator on SOI waveguide," *Opt. Exp.*, vol. 22, no. 12, pp. 15292–15297, Jun. 2014.

[25] J. Gosciniak and D. T. Tan, "Graphene-based waveguide integrated dielectric-loaded plasmonic electro-absorption modulators," *Nanotechnology*, vol. 24, no. 18, Apr. 2013, Art. no. 185202.

[26] X. Hu and J. Wang, "High figure of merit graphene modulator based on long-range hybrid plasmonic slot waveguide," *IEEE J. Quantum Electron.* vol. 53, no. 3, Jun. 2017, Art. no. 7200308.

[27] M. Fan, H. Yang, P. Zheng, G. Hu, B. Yun, and Y. Cui, "Multilayer graphene electro-absorption optical modulator based on double-stripe silicon nitride waveguide," *Opt. Exp.*, vol. 25, no. 18, pp. 21619–21629, Sep. 2017.

[28] D. A. Kuzmin, I. V. Bychkov, and V. G. Shavrov, "Influence of graphene coating on speckle-pattern rotation of light in gyrotropic optical fiber," *Opt. Lett.*, vol. 40, no. 6, pp. 890–893, Mar. 2015.
[29] J. Wang *et al.*, "High-responsivity graphene-on-silicon slot waveguide photodetectors," *Nanoscale*, vol. 8, no. 27, pp. 13206–13211, Jul. 2016.
[30] Q. Bao and K. P. Loh, "Graphene photonics, plasmonics, and broadband optoelectronic devices," *ACS Nano*, vol. 6, no. 5, pp. 3677–3694, May 2012.
[31] T. Stauber, N. M. R. Peres, and A. K. Geim, "The optical conductivity of graphene in the visible region of the spectrum," *Phys. Rev. B*, vol. 78, no. 8, Aug. 2008, Art. no. 085432.
[32] L. A. Shiramin and D. V. Thourhout, "Graphene modulators and switches integrated on silicon and silicon nitride waveguide," *IEEE J. Sel. Topics Quantum Electron.*, vol. 23, no. 1, Jan./Feb. 2017, Art. no. 3600107.
[33] W. Lin, L. Wei, and J. Xunya, "Tunable control of electromagnetically induced transparency analogue in a compact graphene-based waveguide," *Opt. Lett.*, vol. 40, no. 10, pp. 2325–2328, May 2015.
[34] Z. Chang and K. S. Chiang, "Experimental verification of optical models of graphene with multimode slab waveguides," *Opt. Lett.*, vol. 41, no. 9, pp. 2129–2132, May 2016.
[35] A. Zunger, A. Katzir, and A. Halperin, "Optical properties of hexagonal boron nitride," *Phys. Rev. B*, vol. 13, no. 12, pp. 5560–5573, Jun. 1976.
[36] N. R. Jungwirth and G. D. Fuchs, "Optical absorption and emission mechanisms of single defects in hexagonal boron nitride," *Phys. Rev. Lett.*, vol. 119, no. 5, Jul. 2017, Art. no. 057401.
[37] Z. Zhong, B. Zhang, H. Chen, D. Huang, and L. Peng, "Realization of low contact resistance close to theoretical limit in graphene transistors," *Nano Res.*, vol. 8, no. 5, pp. 1669–1679, Mar. 2015.
[38] Z. Cheng *et al.*, "Focusing subwavelength grating coupler for mid-infrared suspended membrane waveguide," *Opt. Lett.*, vol. 37, no. 7, pp. 1217–1219, Mar. 2012.
[39] P. Alberto, M. J. Cryan, J. G. Rarity, Y. Siyuan, and J. L. O'Brien, "Silica-on-silicon waveguide quantum circuits," *Science*, vol. 320, no. 5876, pp. 646–649, May 2008.
[40] C. T. Phare, Y. H. D. Lee, J. Cardenas, and M. Lipson, "Graphene electro-optic modulator with 30 GHz bandwidth," *Nature Photon.*, vol. 9, no. 8, pp. 511–514, Jul. 2015.
[41] J. Meng *et al.*, "Synthesis of in-plane and stacked graphene/hexagonal boron nitride heterostructures by combining with ion beam sputtering deposition and chemical vapor deposition," *Nanoscale.*, vol. 7, no. 38, pp. 16046–16053, Mar. 2016.
[42] W. Gannett, W. Regan, K. Watanabe, T. Taniguchi, M. F. Crommie, and A. Zettl, "Boron nitride substrates for high mobility chemical vapor deposited graphene," *Appl. Phys. Lett.*, vol. 98, no. 24, Jul. 2011, Art. no. 242105.
[43] P. J. Zomer, S. P. Dash, N. Tombros, and B. J. V. Wees, "A transfer technique for high mobility graphene devices on commercially available hexagonal boron nitride," *Appl. Phys. Lett.*, vol. 99, no. 23, Oct. 2011, Art. no. 232104.
[44] Y. Ding *et al.*, "Efficient electro-optic modulation in low-loss graphene-plasmonic slot waveguides," *Nanoscale*, vol. 9, no. 40, pp. 15576–15581, Sep. 2017.
[45] J. Yan, Y. Zhang, P. Kim, and A. Pinczuk, "Electric field effect tuning of electron-phonon coupling in graphene," *Phys. Rev. Lett.*, vol. 98, no. 16, Apr. 2007, Art. no. 166802.
[46] F. Wang *et al.*, "Gate-variable optical transitions in graphene," *Science*, vol. 320, no. 5873, pp. 206–209, Mar. 2008.
[47] C. Hwang *et al.*, "Fermi velocity engineering in graphene by substrate modification," *Sci. Rep.*, vol. 2, Aug. 2012, Art. no. 590.
[48] Y. J. Y. Gwan *et al.*, "Electron tunneling through atomically flat and ultrathin hexagonal boron nitride," *Appl. Phys. Lett.*, vol. 99, no. 24, Dec. 2011, Art. no. 243114.
[49] V. R. Almeida, X. Qianfan, C. A. Barrios, and L. Michal, "Guiding and confining light in void nanostructure," *Opt. Lett.* vol. 29, no. 11, pp. 1209–1211, Jun. 2004.
[50] W. Yu, K. Mei, Y. Xu, and Z. Zhou, "Analysis of scattering loss due to sidewall roughness in slot waveguides by variation of mode effective index," *J. Opt.*, vol. 20, Jan. 2018, Art. no. 025801.
[51] A. Li, T. Vanvaerenbergh, P. Deheyn, P. Bienstman, and W. Bogaerts, "Backscattering in silicon microring resonators: A quantitative analysis," *Laser Photon. Rev.*, vol. 10, no. 3, pp. 420–431, May 2016.
[52] K. K. Lee, D. R. Lim, L. C. Kimerling, J. Shin, and F. Cerrina, "Fabrication of ultralow-loss Si/SiO(2) waveguides by roughness reduction," *Opt. Lett.*, vol. 26, no. 23, pp. 1888–1890, Dec. 2001.
[53] M. C. M. Lee and M. C. Wu, "Thermal annealing in hydrogen for 3-D profile transformation on silicon-on-insulator and sidewall roughness reduction," *J. Microelectromech. Syst.*, vol. 15, no. 2, pp. 338–343, Apr. 2006.
[54] S. Haishan, C. Antao, A. Don, S. Attila, and R. S. Kim, "Reduction of scattering loss of silicon slot waveguides by RCA smoothing," *Opt. Lett.*, vol. 37, no. 1, pp. 13–15, Dec. 2012.
[55] T. Alasaarela *et al.*, "Reduced propagation loss in silicon strip and slot waveguides coated by atomic layer deposition," *Opt. Exp.*, vol. 19, no. 12, pp. 11529–11538, May 2011.
[56] A. Säynätjoki *et al.*, "Low-loss silicon slot waveguides and couplers fabricated with optical lithography and atomic layer deposition," *Opt. Exp.*, vol. 19, no. 27, pp. 26275–26282, Dec. 2011.
[57] D. Ran *et al.*, "Low-loss strip-loaded slot waveguides in silicon-on-insulator," *Opt. Exp.*, vol. 18, no. 24, pp. 25061–25067, Nov. 2010.
[58] T. Baehr-Jones, M. Hochberg, C. Walker, and A. Scherer, "High-Q optical resonators in silicon-on-insulator-based slot waveguides," *Appl. Phys. Lett.*, vol. 86, Feb. 2005, Art. no. 081101.
[59] T. Fang, A. Konar, H. Xing, and D. Jena, "Carrier statistics and quantum capacitance of graphene sheets and ribbons," *Appl. Phys. Lett.*, vol. 91, Aug. 2007, Art. no. 092109.
[60] S. J. Koester and M. Li, "High-speed waveguide-coupled graphene-on-graphene optical modulators," *Appl. Phys. Lett.*, vol. 100, Apr. 2012, Art. no. 171107.
[61] Y. Hu *et al.*, "High-speed silicon modulator based on cascaded microring resonators," *Opt. Exp.*, vol. 20, no. 14, pp. 15079–15085, Jun. 2012.
[62] A. C. Ferrari, "Graphene photonics and optoelectronics," *Nature Photon.*, vol. 4, no. 9, pp. 611–622, Aug. 2016.